Korean J. Chem. Eng., 39(8), 2010-2019 (2022)
DOI: 10.1007/s11814-022-1171-7

pISSN: 0256-1115
eISSN: 1975-7220

Experimental study on CO_2 bubble dynamics under different solution viscosity and absorbent concentration

Yang Jia-xi, Gao Dan†, Qi You-wei, and Zhang Heng

North China Electric Power University, Beijing 102206, China
(*Received 4 February 2022 • Revised 8 April 2022 • Accepted 11 May 2022*)

Abstract−Carbon dioxide (CO_2) emitted by fossil energy combustion is related to the greenhouse effect. To further study the motion dynamics of CO_2 bubbles in various solutions so as to better absorb them, a CO_2 bubble experimental platform was built. The growth and motion of a single CO_2 bubble were experimented in five concentrations of NaOH, $NaHCO_3$ solutions and five viscosity deionized waters, photographed with a high-speed camera and imported into PyCharm for analysis. Based on this, four kinds of CO_2 bubbles were experimentally studied. The results show that the viscosity leads to the increase of rising time; the maximum rise time is 0.518 s when the viscosity is 100 mPa·s, the aspect ratio δ of CO_2 bubble in solution, there will be an "L" distribution, and the minimum rise time is close to rising after the bubble is separated from the injector. $NaHCO_3$ inhibits the reaction between NaOH solution and CO_2, resulting in the cross-section ratio κ change decreasing. The concentration of NaOH solution most conducive to CO_2 absorption is 0.039 g/ml and 0.058 g/ml.

Keywords: CO_2 Bubble, Rise Time, Aspect Ratio, Cross-section Ratio

INTRODUCTION

Since the industrial revolution, the amount of Carbon Dioxide (CO_2) that has been released into the atmosphere has produced a significant impact on global climate change [1-4]. This is mainly due to the inevitable production of CO_2 gas caused by the burning of fossil energy. CO_2 gas has excellent heat absorption and insulation functions. Due to its increase in the atmosphere, an invisible glass cover is formed. The heat radiated from the sun cannot be transferred to outer space, so the average surface temperature rises [5]. At the same time, excessive CO_2 will also generate acid rain and other phenomena, putting people's production and life in danger. On this basis, countries all over the world are increasingly focusing on carbon capture, utilization and storage (CCUS) technology, which involves capturing and purifying the carbon dioxide emitted in the production process before reusing it in a new production process. In this way, carbon dioxide is recycled, environmentally friendly and economically maximized. At present, pre-combustion capture, oxygen-enriched combustion and post-combustion capture are the basic components of CCUS [6]. Post-combustion capture technology is considered to be the most feasible CO_2 capture method because it can meet the requirements of existing flue gas characteristics with small quantities. Capture after combustion can be divided into solvent absorption method, an adsorption method, membrane separation method and low temperature separation method [7]. At present, the solvent absorption method, which mainly transports CO_2 bubbles into the absorbent, is the most widely used method. Therefore, many scholars have studied CO_2 bubbles. As early as 1851, Stokes [8] began to study the gas motion equation in pure water. After that, Rodrigue [9] further deduced the bubble motion after considering the liquid viscosity, and obtained the correlation of resistance coefficient and velocity coefficient in the rising process of a bubble. After that, Li [10] studied the mass transfer of CO_2 bubbles in the liquid phase. The experimental results showed that the volumetric mass transfer coefficient increased with the increase of gas flow and decreased with the increase of liquid concentration.

In 1990, Hsunling [11] proposed using ammonia as an absorbent to capture CO_2. Because a power plant needs to use a large amount of ammonia solution during denitration, the equipment transformation and the operation are relatively simple. However, ammonia is extremely volatile. It will volatilize quickly if heated in the capture process, which is easy to cause secondary pollution to the environment [12,13]. As a result, in recent years, the research on CO_2 absorbent has changed with each passing day. Garcia [14] found that it can reduce the partial pressure of CO_2 and improve its solubility by adding organic soluble alcohol to organic amine aqueous solution instead of part of water. Li et al. [15] mixed and prepared multiphase D30P30H40 solvent for CO_2 absorption. According to the findings, more than 90% of CO_2 in this solution can be enriched in the low phase region. At the same time, 1-propanol as a suitable medium can accelerate the phase separation and promote the reaction between mixed solvent and CO_2. Niegodajew et al. [16] used the two-fluid Euler Model in CFD to simulate a 30% monoethanolamine (MEA) solution. When the MEA concentration is high enough, the capture efficiency mainly depends on the content of CO_2. Adding solvent into the membrane to further capture CO_2 has also become one of the research hotspots in recent years. Kofal, Ansaloni, Xu and others [17-19] have prepared porous composite membranes for CO_2 capture. It was found during

†To whom correspondence should be addressed.
E-mail: gaodan@ncepu.edu.cn

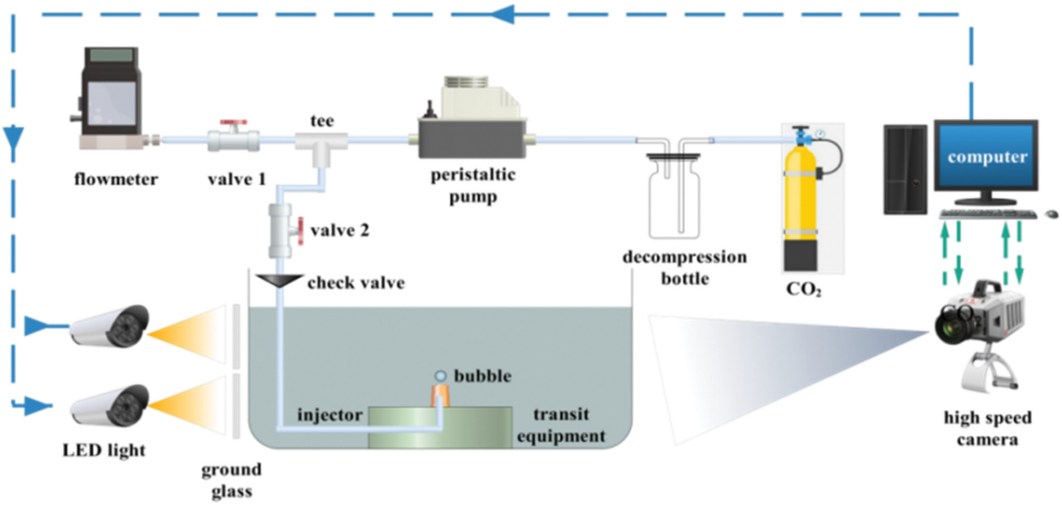

Fig. 1. Schematic diagram of CO_2 visualization experimental platform.

the experiment that adding absorbent into the composite membrane can also improve the recovery of CO_2. Nilavuckkarasi et al. [20] used ultrasonic technology to treat MEA after CO_2 capture in low temperature environment, and found that the loss rate can be reduced by more than 8%.

At the same time, although solid substances are used to capture CO_2 in CCUS, compared with liquid CO_2 capture, the resistance of equipment is small and the waste is easy to transport, solid substances are expensive and have low absorption capacity. There are many studies on solid CO_2 capture. To reduce the cost, Pevida et al. [21] used a melamine-formaldehyde resin as a raw material to prepare nitrogen-rich carbon porous adsorption solid with high porosity. The experiment found that the adsorption capacity of CO_2 reaches 2.25 mmolg at 25 °C. Ke Wang et al. [22] found that Li_4SiO_4 combined with slow burning glucose can be used to adsorb high-temperature and low concentration CO_2 gas, and the maximum absorption capacity reaches 35.0% at 580 °C. Wang et al. [23] studied modified MgO and discovered that adding glutamic acid as a combustion additive can reduce the grain size of MgO, expose more alkaline adsorption active sites and make MgO more conducive to CO_2 adsorption. Tian [24] prepared calcium based CO_2 adsorption material with steel slag as raw material, to recycle calcium and iron in steel slag while reducing CO_2 in iron and steel industry. Silva et al. [25] modified MCM-41 by carbon deposition pickling and applied it to carbon dioxide adsorption. When compared with the original MCM-41, the CO_2 adsorption capacity has been greatly improved after synthetic treatment.

Many scholars have done considerable research on CO_2 recovery and capture, especially in the types of solvents, the improvement of amines and alcohols and gas-solid multiphase substances. However, the dynamics of CO_2 bubbles in the solvent recovery process still needs to be further studied. Therefore, it is proposed to build a visual experiment platform and use a high-speed camera to capture the dynamics of CO_2 bubbles in NaOH and $NaHCO_3$ solutions with different concentrations, as well as deionized water with different viscosity. The innovation is the dynamics of CO_2 bubble in the solutions are studied, a visual experimental platform is built, the effects of different viscosity and solutions are analyzed, the optimal absorption concentration of NaOH solution is obtained. Finally, a reference for improving the capture rate is provided.

1. Experimental Platform Construction and Main Instrument Parameters

1-1. Experimental Platform Construction

CO_2 is the main greenhouse gas, accounting for about 0.03% of the total atmospheric capacity. To improve solvent absorption efficiency and realize carbon dioxide recycling better and faster, it is necessary to understand its motion characteristics in different solutions. A CO_2 bubble visualization experiment platform was built based on the features of CO_2 and common solutions, and the specific schematic diagram is shown in Fig. 1. The principle of the visual experiment platform mainly relies on the reaction of citric acid and baking soda in the CO_2 bubble generation bottle to generate pure CO_2 gas. The CO_2 gas enters the bottom of the bottle through the pressure-reducing bottle. The CO_2 gas can maintain constant pressure in the pressure-reducing bottle and discharge the remaining air in the bottle. When the pressure is too high, the rubber plug on the upper part of the pressure-reducing bottle will pop up automatically to ensure the experiment's safety and accuracy. The gas reaches a tee after passing through the outlet of the peristaltic pump. The tee can finely adjust the gas flow when the pump flow is known and changeable. 3D printing technology is used to create the transit equipment at the bottom of the acrylic cylinder. There is a flow channel for CO_2 gas flow inside, and the upper part has an M6 thread, allowing injectors with different diameters to be replaced conveniently.

1-2. Main Instrument Parameters

The main experiment instruments and parameters constituting the experimental platform are shown in Table 1, and the physical drawing of the experimental platform is shown in Fig. 2. After the CO_2 bottle generates pure CO_2 gas, the CO_2 gas is transmitted to the injector at the bottom of the water cylinder through the peristaltic pump, and the CO_2 bubble is generated by the injector. In the experiment, the clarified lime water is used to inspect the gas at the injector [26]. Until the clarified lime water becomes turbid,

Table 1. Main experimental instruments and parameters

Name	Manufacturer	Parameter
High-speed camera	Fuhuang Junda Co., Ltd-Revealer	Max FPS 60000
LED light	Zhongguan Digital Co., Ltd	Power 200 W
Peristaltic pump	Kamoer Co., Ltd	Maximum flow 14 mL/min
Acrylic water tank	-	Volume 15×15×15 cm
Filter	Huashang laser Co., Ltd	Transmission wavelength 400-700 nm
CO_2 bubble generation bottle	ZRDR Co., Ltd	Capacity 1L
Switching device	-	Volume 3×3×3 cm

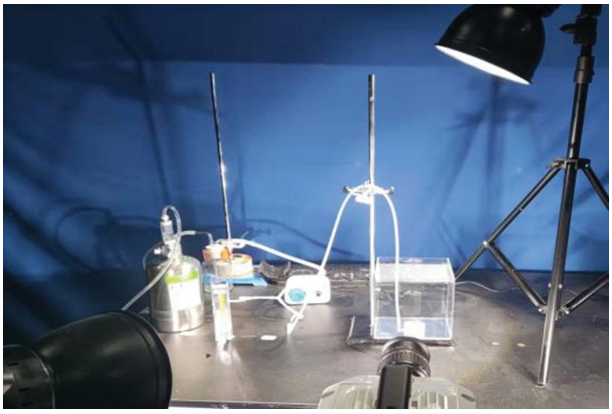

Fig. 2. Physical drawing of experimental platform.

it is considered that the decompression bottle contains only pure carbon dioxide and there is no air left in the whole flexible tube.

The injector and transit equipment are placed at the center of the acrylic water cylinder's bottom, so that the bubbles are not affected by the wall. The computer controls the LED lamp to keep the brightness unchanged as the supplementary light source for the solution. At the same time, the computer also controls the high-speed camera for shooting and data storage, to ensure the accurate recording of transient changes in the process of CO_2 bubble generation and rise.

2. CO_2 Bubble Dynamics Experiment in Different Solutions

With the progress of modern science and technology, high-tech equipment such as high-speed camera, electron microscopes and particle size analyzers are used to study the microbubble movement, which enriches the experimental results. In this experiment, a high-speed camera is utilized to capture the dynamic process of CO_2 bubble growth and movement, allowing for accurate and timely recording of transient changes. First, deionized water is experimented and studied. At 20 (±1) °C, after ensuring that there is no air in the pipe, the peristaltic pump is set to 80% (11.2 ml/min). Then the valve is adjusted to keep the flow meter to 5.0 ml/min constant. At this time, the CO_2 can be produced easily in the deionized water and the flow rate is uniform.

In the experiment, the inner diameters are 0.1 mm, 0.3 mm, 0.5 mm and 1.0 mm, respectively. The CO_2 bubble of the injector will expand to the maximum at the last moment before leaving the injector during the expansion process, and this moment will be taken as the first experiment record point. After that, the CO_2 bubble moves upward from the injector, and the rising CO_2 bubble is photographed and recorded at the same time interval (14.7 μs) until the bubble reaches the liquid level. The injector inside diameter of (a)-(d) in the diagram is 0.1 mm, 0.3 mm, 0.5 mm, and 1.0 mm, respectively. The pictures of the first experiment recording point under four injector radii taken in deionized water are shown in Fig. 3. In the figure, (a)-(d) are 0.1 mm, 0.3 mm, 0.5 mm and 1.0 mm, respectively. It can be seen that the bubbles will be stretched and deformed due to the gravitational effect of the injector in the bubbles.

2-1. Aqueous Solutions of NaOH and $NaHCO_3$ with Different Concentrations

To further study the kinetics of CO_2 bubble in solution, NaOH aqueous solution which is easy to react with it and $NaHCO_3$ aqueous solution, which will not react are selected for further study. NaOH aqueous solution can react violently and quickly with CO_2 gas according to the chemical equations of Eqs. (1) and (2) to produce $NaHCO_3$. Therefore, it is frequently considered as one of the efficient inorganic CO_2 absorbers [27]. In this experiment NaOH aqueous solution with mass concentrations is 0.019 g/ml, 0.039 g/ml, 0.058 g/ml, 0.078 g/ml and 0.097 g/ml, respectively. The flow rate and injector inner diameter are consistent with those in deion-

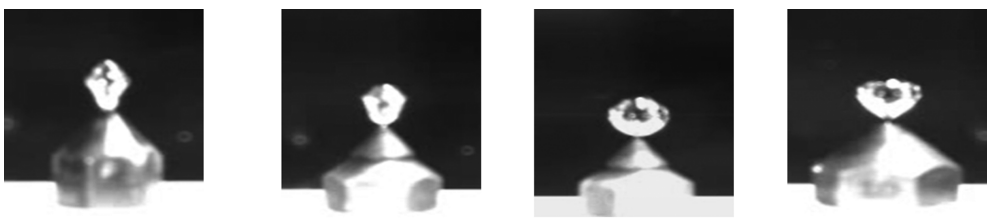

(a) (0.1mm) (b) (0.3mm) (c) (0.5mm) (d) (1.0mm)

Fig. 3. Image of CO_2 bubble in deionized water leaving the injector.

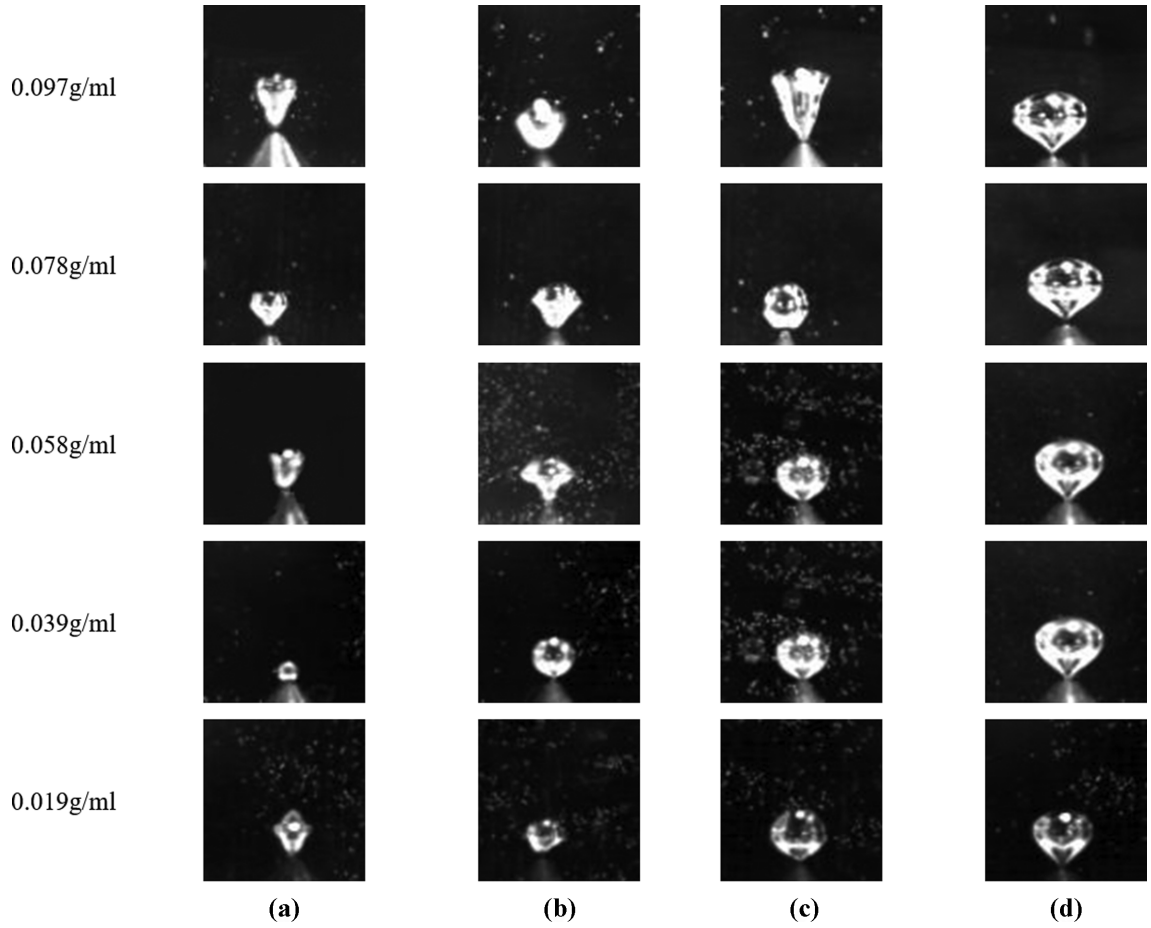

Fig. 4. Image of CO_2 bubble in NaOH solution leaving the injector.

ized water. When other conditions remain unchanged, the first experimental recording point under five concentrations can be captured by using a high-speed camera, as shown in Fig. 4.

$$2NaOH+CO_2 \rightarrow Na_2CO_3+H_2O \quad (1)$$

$$Na_2CO_3+H_2O+CO_2 \rightarrow 2NaHCO_3 \quad (2)$$

Since the final product of the above reaction is $NaHCO_3$, to verify whether a large amount of $NaHCO_3$ wrapped around the CO_2 bubble has an impact on its movement, the CO_2 bubble is further experimented in the $NaHCO_3$ solution with mass concentrations of 0.019 g/ml, 0.039 g/ml, 0.058 g/ml, 0.078 g/ml and 0.097 g/ml under the same other conditions.

2-2. CMC and Oil Solutions with Different Viscosities

To explore the effect of viscosity on cavitation bubbles, sodium carboxymethyl cellulose (NaCMC or CMC for short) is used, which is a white translucent powder (as shown in Fig. 5) with a simplified molecular formula of $[C_6H_7O_2(OH)_2OCH_2COONa]_n$. The CMC aqueous solution is viscous and is a typical non-Newtonian fluid (power-law fluid) [28-31]. When the pH value of the CMC solution is between 2-10, the properties of the CMC solution are relatively stable.

Due to the high viscosity of CMC solution in the experiment, it is necessary to prolong the stirring time to guarantee the full dissolution of CMC. Simultaneously, to eliminate the small bubbles generated by stirring in CMC solution, the standing time also needs to be increased. So after weighing the CMC with an electronic balance, place the CMC in a beaker and add hot water, stir continuously for 12 h and stand for 12 h. The viscosity of a viscometer is adjusted to 20, 40, 60, 80 and 100 mPa·s, respectively, and then

Fig. 5. CMC powder.

Table 2. Measurement degree of uncertainties

Measured parameters	Degree of uncertainty (±)
Temperature	1 °C
CO_2 gas flow	0.05 ml/min
Liquid weight	0.1 g
Gas purity	≥99%
Purity of chemical materials	≥99%
Equipment leakage	≤0.01 ml/min

stand for more than 1 h before the experiment. At the same time, the experiment is carried out again with special engine oil for further comparison.

2-3. Experimental Analysis of Uncertainties

The experimental uncertainties are caused by systematic errors, random errors and gross errors according to the nature and causes. Due to these inevitable reasons, the experiment may be affected. For example, the pump cannot discharge the same volume of gas uniformly, so there will be a certain volume deviation between the bubbles, CO_2 gas may contain other substances (such as trace air) due to equipment leakage; some small errors may be caused by the insufficient equipment precision or measuring range; and the liquid temperature might change slightly when the ambient temperature changes. These uncertainties are summarized in Table 2. It can be seen that these uncertainties account for a small proportion compared with the experiments, so they can be ignored in the case of multiple measurements and careful calibration.

3. Analysis of Experimental Results

To more intuitively and conveniently analyze the CO_2 bubble dynamics in the above experiments, the section ratio is proposed, and the aspect ratio of the cavitation bubble is employed for quantitative analysis [32-34]. The aspect ratio δ represents the ratio of the maximum longitudinal length to the maximum transverse length of CO_2 bubbles (Eq. (3)). The section ratio κ represents the ratio of the cross-sectional area of the bubble to the area at the maximum initial radius (Eq. (4)).

$$\delta = \frac{L_{Z\cdot MAX}}{L_{H\cdot MAN}} \tag{3}$$

$$\kappa = \frac{S_R}{S_0} = \frac{\pi \cdot d_R^2}{\pi \cdot d_0^2} = \sqrt{\frac{d_R}{d_0}} \tag{4}$$

where, δ represents the aspect ratio, which is the ratio of the longest value $L_{Z\cdot Max}$ in the vertical direction to the longest value $L_{H\cdot Max}$ in the horizontal direction, with the unit of 1; κ representative section ratio, 1; S_R is the cross-sectional area at a certain time, m^2, S_0 is the cross-sectional area at the maximum initial radius, m^2; d_R and d_0 are the longest horizontal values at the corresponding time, m; γ represents the deformation rate, %.

To accurately analyze these two parameters, PyCharm Community Edition is used for editing, to accurately identify various parameters of the CO_2 bubble. This process can be divided into 9 steps as shown in Fig. 6: original image, gray processing, binarization, image filling, image expansion, image corrosion, canny edge detection, reverse color and image reverse color. The outline of the CO_2

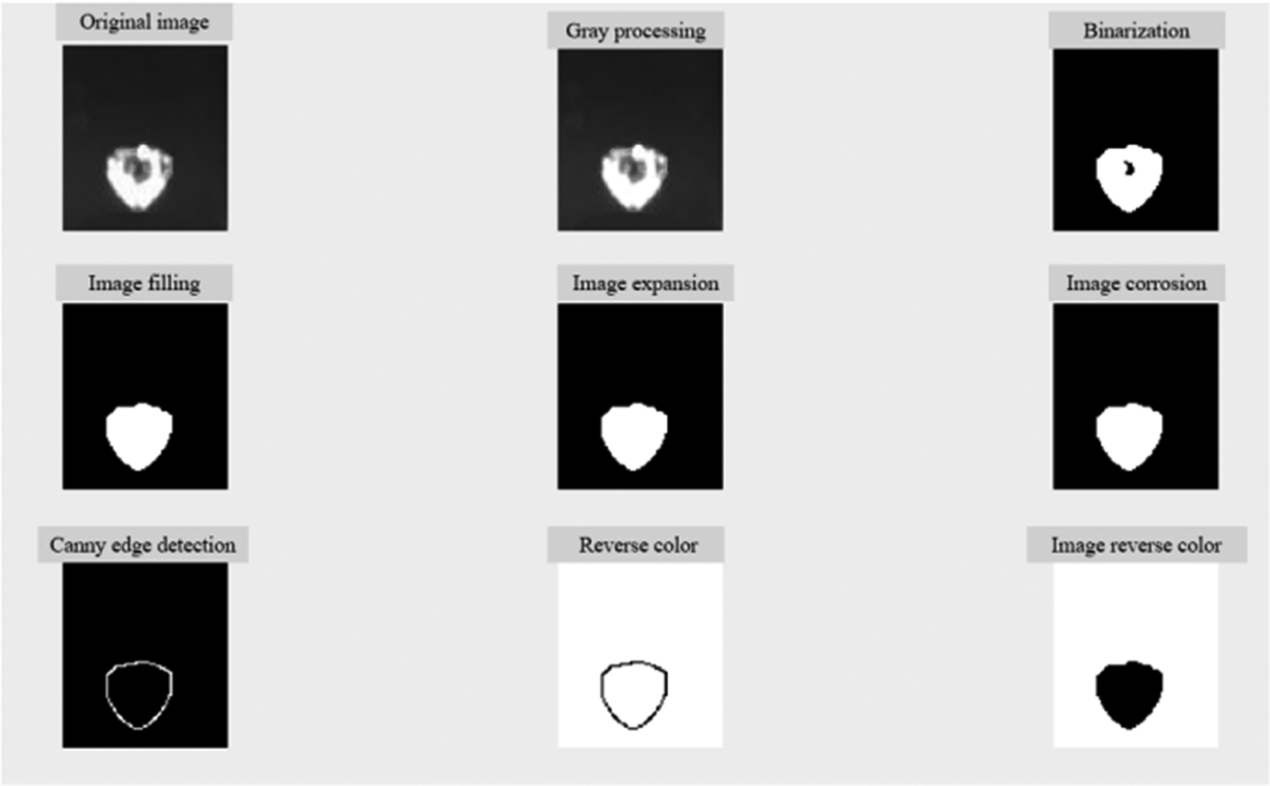

Fig. 6. Image processing based on PyCharm.

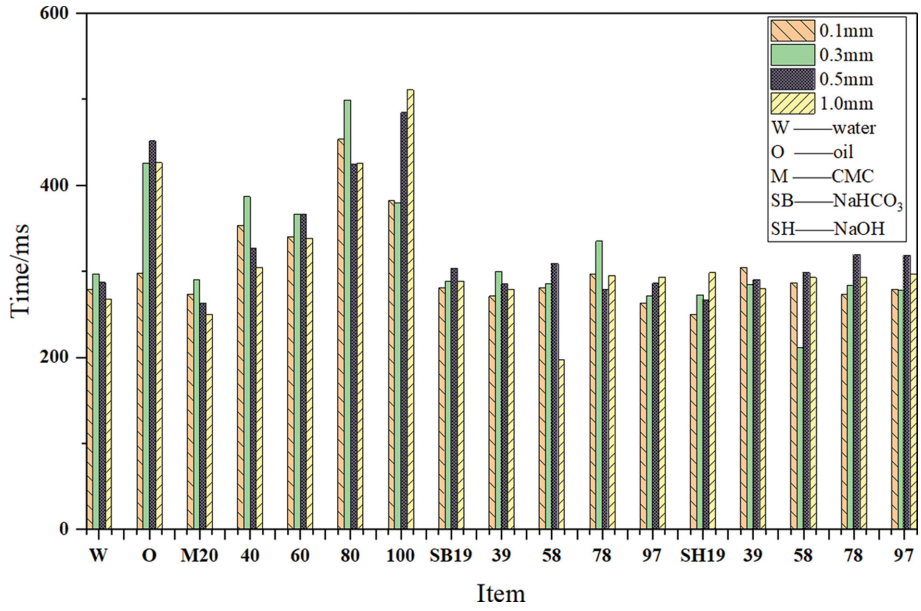

Fig. 7. CO_2 bubble rise time.

bubble can be seen after the reverse color is output, but the bubble is filled with CO_2 gas, in order to obtain the cross section of the CO_2 bubble clearly, the image reverse color is further processed.

Finally, the section as shown in Eq. (5), the longest value in the vertical direction (Eq. (6)) and horizontal direction (Eq. (7)) are calculated by the self-designed program.

$$D=\sum_{i=1}^{n}P_i \tag{5}$$

$$L_{Z\cdot MAX}=\sum_{i=1}^{n}P_{iZ} \tag{6}$$

$$L_{H\cdot MAX}=\sum_{i=1}^{n}P_{iH} \tag{7}$$

where, D is the sectional area, mm^3; $L_{Z\cdot MAX}$ is the length in the vertical direction, mm; $L_{H\cdot MAX}$ is the height in the horizontal direction, mm; P_i is the pixel.

3-1. Rise Time of CO_2 Bubble in Solution

As can be seen from Fig. 7, among the four solutions of deionized water, CMC 40-80 solution and $NaHCO_3$ concentration of 0.039 g/ml and 0.078 g/ml, the CO_2 bubble with injector inner diameter of 0.3 mm has the slowest rising speed, the longest rising time and the maximum time length of 0.498 s.

From Fig. 7 as a whole, the bubble rise time increases with the increase of viscosity. When the viscosity is 100 mPa·s, the CO_2 bubble generated by the 1.0 mm injector rises the slowest, with a maximum rise time of 0.518 s. Compared with deionized water, the bubbles rise time generated by the four injectors increased by 26.9%, 21.7%, 40.7% and 47.6%, respectively. This is mainly due to the increase of the internal viscous force of liquid and the force of liquid molecules. In this case, in bubbles the upward forces such as buoyancy and surface tension are weakened.

3-2. Change of CO_2 Bubble Aspect Ratio in Solution

As can be seen from Fig. 8, the aspect ratio δ will be an "L" distribution when the inner diameter of the injector is 0.1 mm, 0.3 mm, 0.5 mm and 1.0 mm. The maximum value occurs when the CO_2 bubble leaves the injector, and the minimum value occurs within a short time thereafter (no more than 73.5 ms). This minimum value is due to the sudden separation at the injector-bubble junction, and the injector will have an upward reaction force F_δ on the bubble. Further, there is an instantaneous upward acceleration on the lower surface of the bubble, which is significantly greater than the sum of other forces on CO_2 (as shown in Fig. 9). Therefore, δ has an obvious declining trend in four injectors, meaning that the CO_2 bubble will be continuously flattened. Finally, after reaching an extreme value, the acceleration gradually disappears and the bubble rebounds rapidly owing to internal pressure, and then rises gradually under the combined action of buoyancy, gravity,

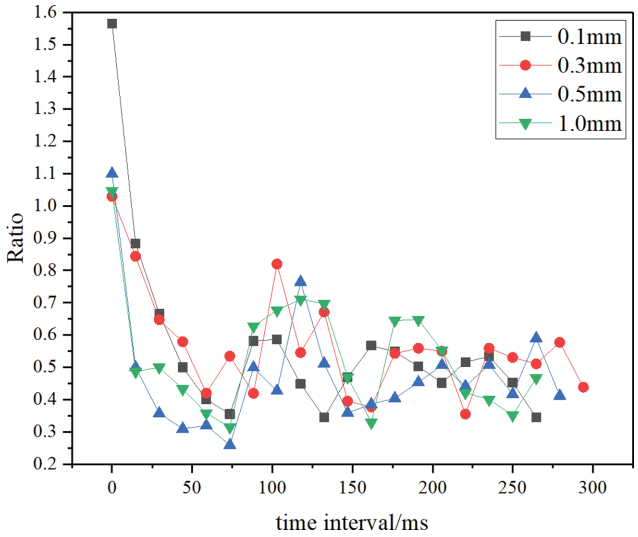

Fig. 8. Aspect ratio of CO_2 bubble in deionized water.

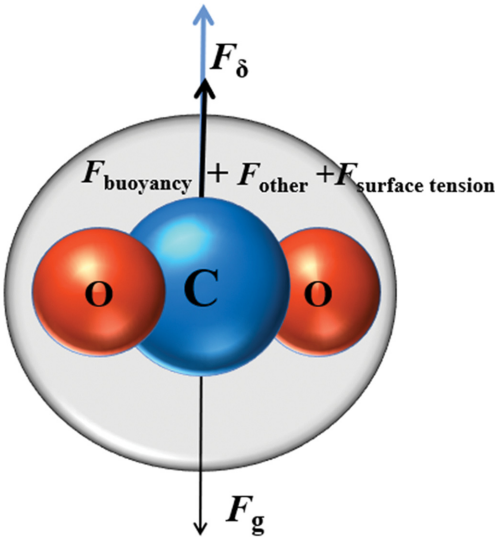

Fig. 9. Stress diagram of CO_2 bubble.

tension and other forces, δ fluctuates in a small range and gradually flattens out. In Fig. 8, since the rising speed of bubbles is different when they reach the liquid level (as shown in Fig. 7), the rising time is also slightly different, resulting in inconsistent end points of the curve.

To further analyze the dynamic characteristics of CO_2 bubbles in NaOH aqueous solution, PyCharm is used to obtain the aspect ratio change shown in Fig. 10. Under-five concentrations of NaOH aqueous solution, the CO_2 bubble separated from the injector δ undergoes an "L" type change, and then a wavy increase and decrease change is formed and gradually tends to be flat. At 0.078 g/ml, the CO_2 bubble is generated when the inner diameter of the injector is 0.1 mm; the δ change trend is not obvious. This is mainly because the reaction rate between CO_2 and NaOH is the fastest at this concentration, and the surrounding $NaHCO_3$ is the greatest. In addition, the solubility of $NaHCO_3$ is less than NaOH, resulting in the change of bubble force, and finally δ is little changed at this stage. The inner diameter of the injector is 1.0 mm during the whole rising stage under the above five concentrations, and the δ always changes

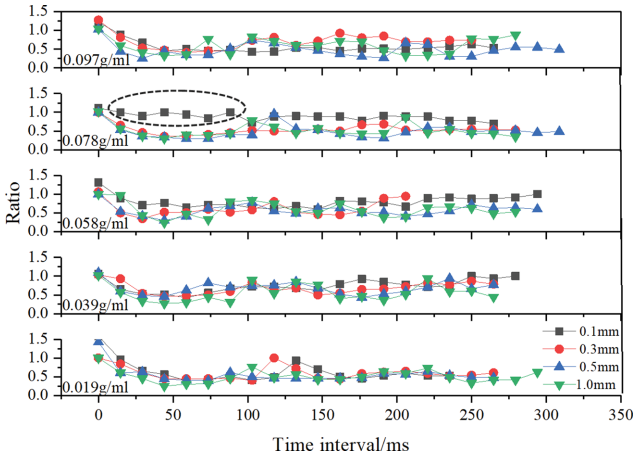

Fig. 10. Aspect ratio of CO_2 bubble in NaOH solution.

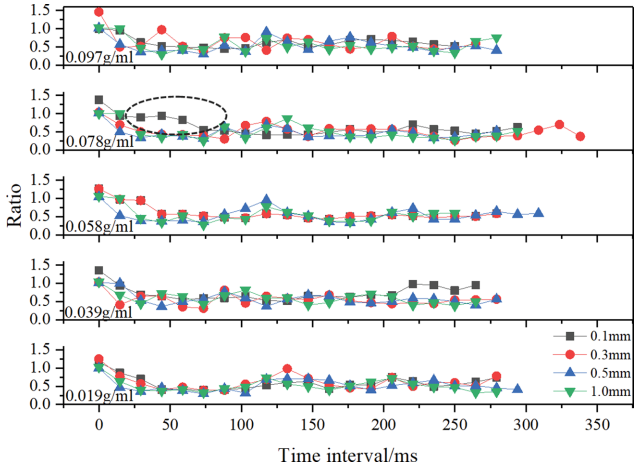

Fig. 11. Aspect ratio of CO_2 bubble in $NaHCO_3$ solution.

little, especially less than deionized water. This is mainly because when the injector radius increases, the initial bubble radius increases. In this case, there is more CO_2 contained in the bubble as a whole, and the internal pressure is relatively stable. At this time, a large amount $NaHCO_3$ is generated by reaction with NaOH which wrapped outside the bubble, resulting in changes in the overall stress. Therefore δ value changes little.

To further verify that wrapping $NaHCO_3$ around the bubble has a great impact on the aspect ratio of the CO_2 bubble in the solution, so as to change the dynamics, the $NaHCO_3$ solution layer is thickened until the whole acrylic cylinder is filled with $NaHCO_3$ liquid, which is obtained by further experiment δ change as shown in Fig. 11. It can be seen that the CO_2 bubble is stable without chemical reaction δ is little changed with NaOH in aqueous solution under the concentration of four $NaHCO_3$ aqueous solutions of 0.019 g/ml, 0.039 g/ml, 0.058 g/ml and 0.097 g/ml.

At 0.078 g/ml, it can be seen in the inner area of the ellipse in Fig. 10 that when the inner diameter of the injector is 0.1 mm,

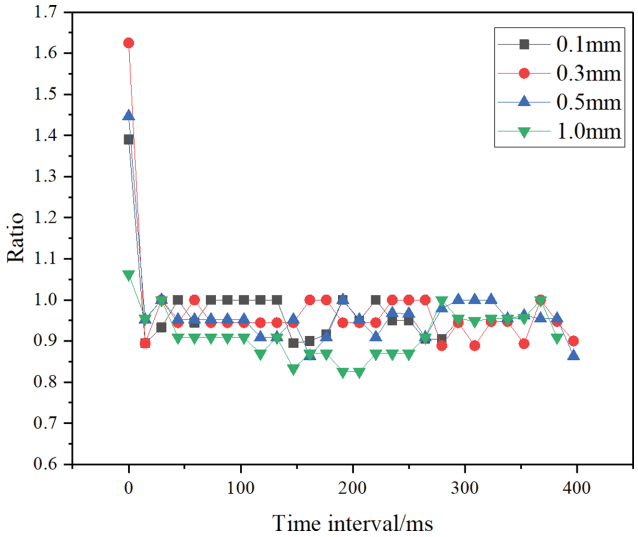

Fig. 12. Aspect ratio of CO_2 bubble in oil.

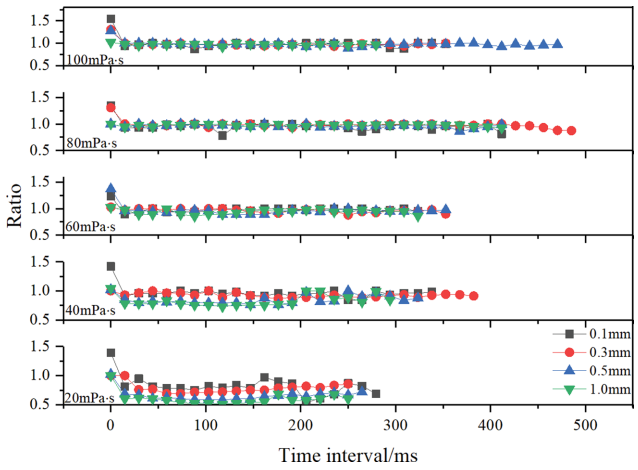

Fig. 13. Aspect ratio of CO_2 bubbles in CMC Solutions with different viscosities.

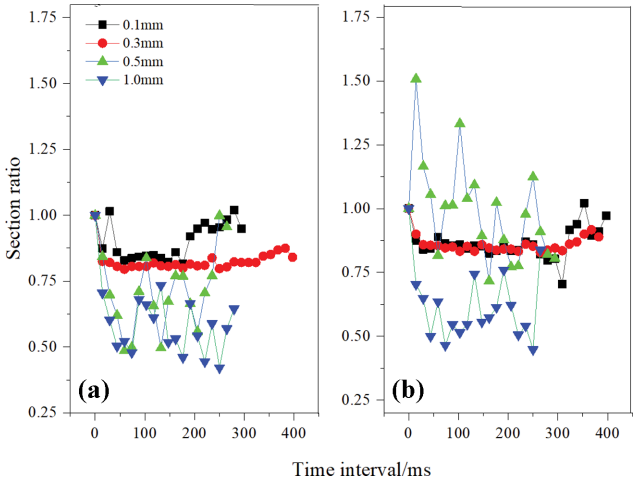

Fig. 14. CO_2 bubble cross-section ratio in oil and deionized water.

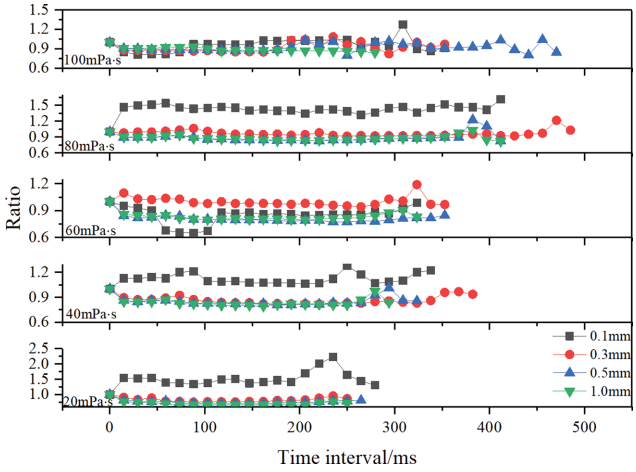

Fig. 15. Cross-section ratio in CMC solution with different viscosity.

CO_2 bubbles of δ change trend is significantly greater than that in deionized water of δ. It is proved that wrapping $NaHCO_3$ will change the overall stress of the bubble, finally resulting in a slight of δ in this stage. Therefore, the fastest production of $NaHCO_3$ in NaOH solution will affect the aspect ratio of small CO_2 bubbles. When the solution viscosity changes, the aspect ratio of CO_2 bubble δ changes in an obvious "L" type . The change of CO_2 bubble in engine oil when the statistical viscosity is 76 mPa·s can be seen in Fig. 12. As can be seen, because of the large viscous force, other external forces on the bubble in the rising process are significantly reduced. The CO_2 bubbles produced by injectors with inner diameters of 0.1 mm, 0.3 mm and 0.5 mm accounted for 66.7%, 78.6%, and 71.4% of the δ points with a value of 1 (±8%) during the whole rising process, respectively. Due to the large amount of gas inside the CO_2 bubble generated by the 1.0 mm injector, it is very easy to cause uneven pressure during the rising process, resulting in uneven stress on the bubble and increased overall deformation. Although δ of change is relatively large, but δ points with a value of 1 (±8%) still account for 35.7% of the whole.

The results of changing the viscosity by CMC for future experiment are shown in Fig. 13. It can be seen that as the increase of viscosity, the viscosity in this process increases value of δ gradually approaches 1, and the deformation of the CO_2 bubble gradually decreases. At this time, the bubble rises continuously in a spherical shape until it reaches the liquid level. When the viscosity is greater than 60 mPa·s, δ changes are small in four injectors.

3-3. Analysis of CO_2 Bubble Section Ratio in Solution

To further study the kinetics of CO_2 in solution, the section ratio is analyzed by Eq. (4). The cross-sectional ratio κ represents the ratio of the area of bubbles after reaction to the initial cross-sectional area, so it is easy to analyze the reaction rate of CO_2. When the reaction is intense, the value of κ decreases obviously, otherwise it is not obvious.

Fig. 14(a) and 14(b) are κ values of CO_2 bubbles in engine oil and deionized water, respectively. It can be seen that during the rise of CO_2 bubble generated by 1.0 mm injector, due to the slow CO_2 dissolution rate, the cross-sectional area changes little. The minimum κ in deionized water is 0.448, while in oil the minimum κ is 0.828. In combination with other situations in Fig. 14, it can be further seen that the increase of viscosity has no effect on CO_2 solubility. The engine oil has an obvious effect on limiting internal gas expansion, the maximum κ is only 1.0 in Fig. 14(a), while the maximum κ reached 1.51 in Fig. 14(b).

In the CMC solution, the cross-section ratio of CO_2 bubbles generated by 0.3 mm, 0.5 mm and 1.0 mm injectors will be significantly inhibited (as shown in Fig. 15). In this case, with the increase in viscosity, the rising speed of bubbles slows, and points will increase at the same rising distance. While the CO_2 bubbles generated by 0.1 mm injectors will be restrained in a small range only when the viscosity is 60 mPa·s.

Among NaOH aqueous solutions that will react violently with CO_2, when the concentration is 0.039 g/ml and 0.058 g/ml, the section ratio κ obviously decreases. The continuous rapid reaction between CO_2 and NaOH results in the continuous decrease of the bubble as a whole. In Fig. 16(c), the minimum κ is only 0.212, and the minimum value in the other four figures is still 0.215 (Fig. 16(e)). When the concentration is low (0.019 g/ml), less NaOH

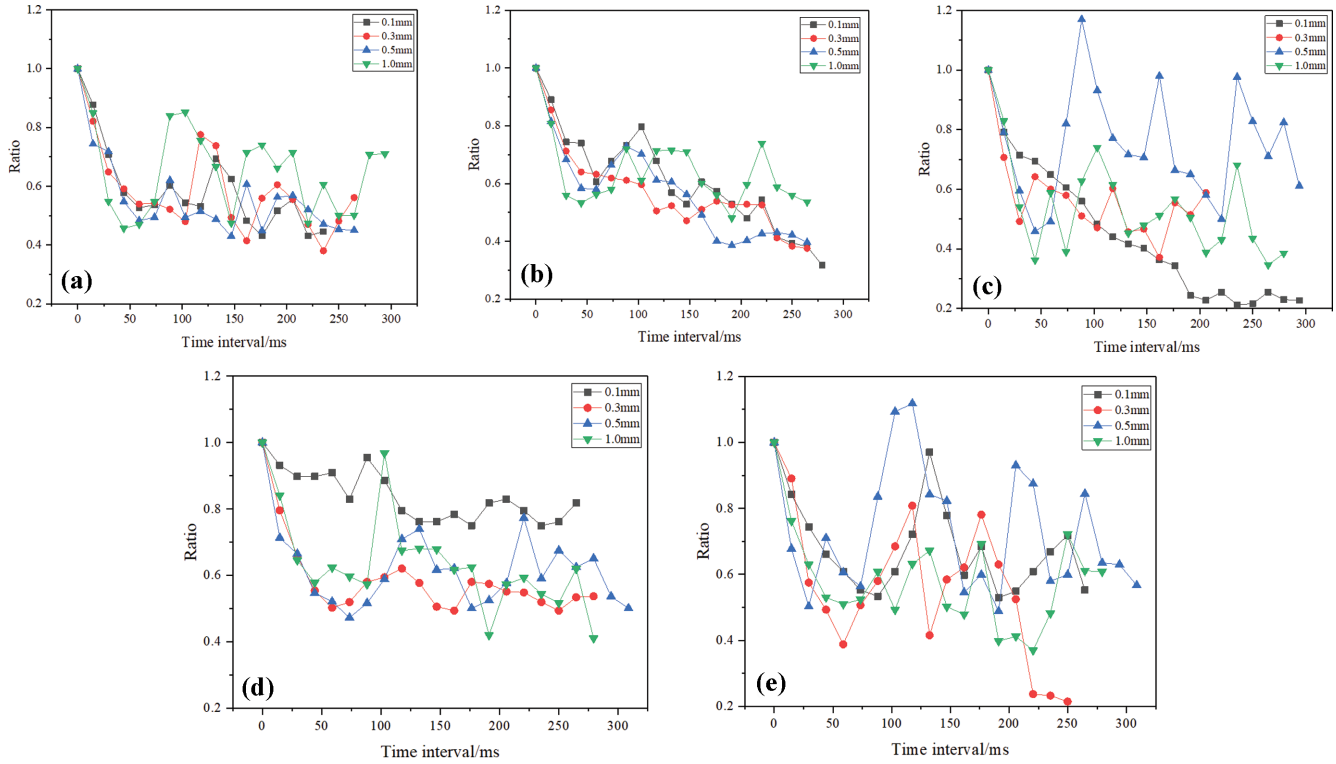

Fig. 16. CO_2 bubble cross-section ratio in NaOH solution.

cannot be supplemented near the bubble surface in time after the reaction consumes NaOH, the κ changes little. When the concentration is too high (0.078 g/ml, 0.097 g/ml), the $NaHCO_3$ generated by the reaction cannot be dissolved quickly, which makes the $NaHCO_3$ concentration around the CO_2 bubble rise continuously and inhibits the occurrence of a chemical reaction. It confirms that $NaHCO_3$ will hurt the CO_2 bubble dynamics.

When CO_2 bubbles move in $NaHCO_3$ solution with concentrations of 0.019 g/ml, 0.039 g/ml, 0.058 g/ml, 0.078 g/ml and 0.097 g/ml, in the same time interval, the κ value can be obtained in Fig. 17. The figure shows that compared with deionized water, the CO_2 bubble generated by 0.1mm inner diameter significantly increases, and the κ of CO_2 bubble produced by the other inner diameters also slightly increases. It can be seen that for CO_2 bubbles produced by injectors with inner diameters of 0.1 mm, 0.3 mm, 0.5 mm and 1.0 mm, it has the largest solubility and the most violent reaction in NaOH solution, followed by deionized water and $NaHCO_3$ solution. When the concentration is 0.039 g/ml and 0.058 g/ml, the solubility of CO_2 bubble is the largest, which is most beneficial to absorption.

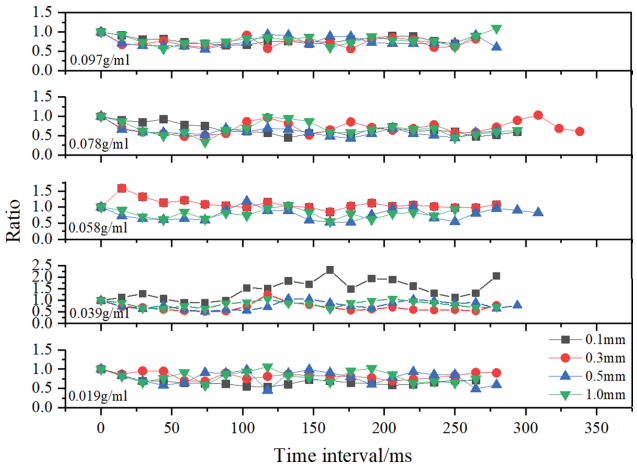

Fig. 17. CO_2 bubble cross-section ratio in $NaHCO_3$ solution.

Therefore, in practical engineering, increasing the viscosity from 1mPa·s to 100 mPa·s can increase the bubble rise time but hinder the bubble deformation. While the $NaHCO_3$ solution and NaOH solution have no effect on the rise time. The influence of the injector with larger inner diameter on the deformation of the CO_2 bubble is limited, but the injector with smaller inner diameter will produce larger deformation, and the change of cross-section ratio is more obvious. Therefore, the 0.1 mm injector should be used when using CO_2 bubble for mass and heat transfer, and absorbing CO_2. At the same time, $NaHCO_3$ will hinder CO_2 absorption. Therefore, NaOH solution with concentration of 0.039 g/ml and 0.058 g/ml is most conducive to CO_2 absorption.

CONCLUSION

The dynamics of the CO_2 bubble reaction in a solvent plays an important role in efficiently reducing carbon emission. Therefore, a visual experimental platform was built. The longitudinal and cross-sectional ratios of CO_2 bubbles in deionized water, engine oil, five solutions of NaOH and $NaHCO_3$ with different concentra-

tions and five Solutions of CMC with different viscosities were analyzed by high-speed camera. The following conclusions were obtained:

(1) The viscosity will increase the rise time of the CO_2 bubble, and the viscosity has the greatest influence on the rise time. At 100 mPa·s, the maximum rise time increases by 41.9% and 47.6%, respectively, compared with the shortest and longest rise time in deionized water.

(2) Aspect ratio of CO_2 bubbles in deionized water, engine oil, NaOH, $NaHCO_3$ solution and CMC solution, the δ will be an "L" distribution, and the minimum value is close to when the bubble continues to rise after leaving the injector.

(3) $NaHCO_3$ will inhibit the reaction between NaOH solution and CO_2, resulting in cross-section ratio κ change being small, and in five concentrations above, the minimum κ value is only 0.212.

(4) According to the aspect ratio and section ratio, it can be obtained that the concentration of NaOH solution most conducive to CO_2 absorption is 0.039 g/ml and 0.058 g/ml.

REFERENCES

1. S. Binet, J. L. Probst, C. B. Guilhe, J. L. Seidel, C. Emblanch and N. Peyraube, *Geochim. Cosmochim. AC*, **270**, 184 (2020).
2. Y. Li, H. Y. Wang, Y. Z. Wang and J. Zhao, *Huadian Technol.*, **43**, 11 (2021).
3. D. Schmidt, C. Yildiz, J. Ströhle and B. Epple, *Fuel*, **284**, 15 (2021).
4. W. Q. Fan, D. Pan, L. Huang and Q. Wang, *Mater. Guide*, **35**, 17 (2021).
5. X. Qian, L. F. Deng, L. F. Wang, R. Shan and H. R. Yuan, *Mater. Guide*, **33**, 11 (2019).
6. M. Xu, X. Zhang, J. L. Fan, G. Lin and D. Xu, *J. Mining Sci.*, **6**, 06 (2021).
7. X. P. Bu, *Clean Coal Technol.*, **20**, 05 (2014).
8. A. Y. Ghalya and M. A. Seddeek, *Chaos Soliton Fract*, **19**, 1 (2004).
9. D. Rodrigue, *Can. J. Chem. Eng.*, **79**, 1 (2001).
10. S. B. Li, Y. G. Ma and T. T. Fu, *Chem. Eng. -New York*, **39**, 10 (2011).
11. H. Bai and A. C. Yeh, *Ind. Eng. Chem. Res.*, **36**, 6 (1997).
12. Y. Wang, Y. Su, W. X. Hou, T. Y. Fan, Y. Y. Xiao, R. Yin, Y. Li and J. Zhao, *Chem. Manage.*, **31**, 19 (2021).
13. C. B. Liu, *Marine Power Technol.*, **41**, 10 (2021).
14. M. Garcia, H. K. Knuutila, U. E. Aronu and S. Gu, *Int. J. Greenh. Gas Con.*, **78**, 11 (2018).
15. X. S. Li, J. Liu, W. F. Jiang, G. Gao, F. Wu, C. Luo, L. Qi and C. Zhang, *Sep. Purif. Technol.*, **275**, 15 (2021).
16. P. Niegodajew and D. Asendrych, *Appl. Math. Model.*, **40**, 23 (2016).
17. M. F. Kofal, A. Mustafa, A. F. Ismail, M. R. DashtArzhandi and T. Matsuura, *J. Nat. Gas Sci. Eng.*, **31**, 4 (2016).
18. L. Ansaloni, A. Hartono, M. Awais, H. K. Knuutila and L. Deng, *Chem. Eng. J.*, **359**, 11 (2018).
19. L. Xu, Y. Qin, L. Liu, J Xiao and Z. Ding, *Korean J. Chem. Eng.*, **38**, 1032 (2021).
20. R. K. Nilavuckkarasi, P. Muthumari and B. Ambedkar, *Chem. Eng. Process*, **151**, 3 (2020).
21. C. Pevida, T. C. Drage and C. E. Snape, *Carbon*, **46**, 11 (2008).
22. K. Wang, F. Gu and P. T. Clough, *Chem. Eng. J.*, **408**, 12 (2020).
23. M. H. Wang, H. M. Liu, Y. L. Xie, S. Gao, J. Ding and Y. X. Wang, *Ion Exchange and Adsorption*, **37**, 04 (2021).
24. G. Falzone, I. Mehdipour, N. Neithalath, M. Bauchy and G. Sant, *AIChE J.*, **67**, 36 (2021).
25. B. Silva, D. Silva and A. Silva, *J. Sol-Gel Sci. Technol.*, **97**, 6 (2021).
26. V. Kolachana, K. Cholkar, W. M. Kayani, G. K. Kouassi and N. M. M. Gowda, *Am. J. Org. Chem.*, **2**(1), 18 (2012).
27. L. Zhang, S. X. Ju, Y. F. Yan and Z. E. Zhang, *J. Chem. Eng.*, **65**, 06 (2014).
28. A. Shadloo, K. Peyvandi and A. Shojaeian, *J. Mol. Liq.*, **347**, 2 (2021).
29. J. Saikiaa, A. Saikiab and D. Saikiac, *Mater. Today*, **09**, 535 (2020).
30. Z. Y. Ding, R. Ding, X. Zheng and X. Chen, *J. Fujian Normal University*, **37**, 06 (2021).
31. Y. J. Shi, X. Y. Wang, Y. Zhang and L. M. Wei, *Micro Nano Electronic Technol.*, **56**, 04 (2019).
32. P. Ritesh and M. S. Kumar, *J. Ind. Eng. Chem.*, **90**, 10 (2020).
33. H. Li, Z. Liu, J. H. Chen, B. J. Sun, Y. L. Guo and H. K. He, *Exp. Therm. Fluid Sci.*, **88**, 11 (2017).
34. A. Shohei, H. Kosuke, H. Shigeo and T. Akio, *Exp. Therm. Fluid Sci.*, **96**, 9 (2018).